Development of highly efficient cost-effective CdS/Ag nanocomposite for removal of azo dyes under UV and solar light

S. Ravikumar [a,d,1], Durai Mani [b,1], E. Chicardi [c], R. Sepúlveda [c], Krishnakumar Balu [c,*], V. Pandiyan [a,**], Young-Ho Ahn [b,***]

[a] Department of Physics, Nehru Memorial College (Autonomous), Puthanampatti Affiliated to Bharathidasan University, Tiruchirappalli, 621007, Tamil Nadu, India
[b] Environmental Science and Engineering Laboratory, Department of Civil Engineering, Yeungnam University, Geongsan, 38541, Republic of Korea
[c] Departamento de Ingeniería y Ciencia de los Materiales y del Transporte, E.T.S. de Ingenieros, Universidad de Sevilla, Avda. Camino de los Descubrimientos s/n., 41092, Sevilla, Spain
[d] Department of Physics, Thanthai Hans Roever College (Autonomous), Perambalur, 621212, Tamil Nadu, India

A B S T R A C T

Water pollution by toxic dyes is an environmental problem that threatens human health. A green technology to solve this problem is the use of highly efficient photocatalysts under visible/solar light to degrade these organic molecules. However, develop affordable photocatalytic particles with high luminescence performance, enhanced stability, and low degradation is still a challenge. Here, it is reported the hydrothermal synthesis of an advanced and cost-effective nanocomposite based on a ceramic, cadmium sulphide, covered by silver nanoparticles (CdS/Ag), with outstanding photocatalytic efficiency for toxic dyes degradation under ultraviolet and direct solar light. The CdS/Ag nanocomposite completely degrade the Reactive Red 120 (RR 120), Acid Black 1 (AB 1) and Direct Blue 15 (DB 15) dyes in both light irradiations. Without scavenger, about 93% of degradation was observed at 75 min, remaining a high stability (more than 90%) after fourth degradation cycles.

1. Introduction

Semiconductor ceramic nanoparticles have attracted keen interest in the photocatalytic degradation of organic molecules due to their unique properties. Nanosized semiconductor ceramic particles possess different physicochemical (electronic, magnetic, biological, electro and optical) properties than the bulk materials [1]. The heterogeneous semiconductor nanoparticle is used to degrade the toxic organic molecules by the advanced oxidation process (AOP) [2–4]. AOP is an efficient and cost-effective method to remove organic molecules without any secondary hazardous, and this method addresses the limitations of the traditional method. The photocatalytic activity of heterogeneous material enhances photo-reactivity and photo-stability. Photocatalysis is an advanced oxidation technology for the removal and pre-treatment of various toxic organic molecules in wastewater. In the photocatalytic reaction in aqueous medium under sunlight and UV light, the generation of hydroxyl radicals and superoxide anions are responsible for the

degradation of organic molecules [5,6].

CdS is one of the important II–VI ceramic semiconductors with excellent luminescence, wide bandgap, and photochemistry properties. The high photo-sensitive nature of CdS advantageous for the photocatalytic reaction to remove the organic pollutants and it is a well-known photocatalyst [7,8]. CdS has the ability to degrade toxic organic compounds due to the wide high absorption range in the electromagnetic spectrum. Deka et al. [9], studied the optical, magnetic, and electrical properties of CdS doping the metal ions to enhance the photocatalytic activity. The photocatalytic activity of the CdS is further enhanced by integrating the co-catalyst [10]. The Ag is a good candidate to enhance the luminescence performance, stability, degradation performance, and functionalization [11]. Moreover, the high photo reactivity of CdS increases the hydrogen generation, while the use similar co-catalyst with wide bandgap (Ag) for the photocatalytic removal of organic molecules increases the charge separation and safeguard the more active catalysts [12]. The strong oxidation power of the CdS

greatly enhance the photocatalytic wastewater treatment. Liu et al. [13] reported the synthesis of heterostructure CdS/Ag and its characterization by a complex hydrothermal method, covering the use of polyvinylpyrrolidone (PVP), sodium sulphide (Na₂S), thiourea and silver nitrate (AgNO₃). Thus, the heterostructure obtained is based on Ag nanowire cores covering by CdS shells.

The present work aims to develop the ceramic cadmium sulphide nanoparticles covered by silver, and its utilization in the degradation of different toxic organic substances under UV-A and solar lights [14–17]. Solar light harvesting related semiconducting materials is a really a challenging task for current research environment [18–20]. Impurity incapacitating is an effective and the most frequently method used to extend the optical absorption edge of wide band gap semiconductors since the developed material is giving to be utilized in UV as well as solar light.

2. Experimental procedure

2.1. Materials and methods

Cadmium acetate dihydrate, thioacetamide, ascorbic acid and silver nitrate, the commercial azo dye Acid Black 1 (AB 1) (CAS No:1064-48-8), and Direct Blue 15 (DB 15) (CAS No: 2429-74-5), were obtained from Sigma-Aldrich. Also, the commercial azo dye Reactive Red 120 (RR 120) was purchased from Balaji Color Company and Auxiliaries (Chennai). The instrumentation details are given in supporting information (see Supporting information).

2.2. Preparation of CdS and CdS/Ag nanocomposite

The hydrothermal method was employed to prepare CdS/Ag nanocomposites (Fig. S1, see Supporting information). Initially, 5.330 g (0.02 M) of cadmium acetate dihydrate was dissolved in 25 mL 1:1 ethanol/water solution at 50 °C. To this, 10 mL of water containing 46 mg of silver nitrate was added and followed by addition of 10 mL water containing 50 mg of ascorbic acid (reducing agent). Then, it was sonicated for 10 min, and followed by stirring. To the above mixture, 25 mL of the solution (1:1, EtOH/H₂O) containing 0.02 M (1.502 g) of thioacetamide was added, and then stirring continued for 3h. After that, the resultant mixture was transferred to autoclave and maintained temperature at 140 °C for 15–20 h. Then, it was filtered, washed with 1:1 EtOH/H₂O mixture and dried in a hot air oven at 90 °C for 5h, and followed by calcinated at 450 °C for 3h in a muffle furnace. This catalyst contains 1 wt% of Ag with respect to CdS. 0.5 and 1.5 wt% of Ag loaded CdS samples were prepared with respective amount of silver nitrate. The bare CdS was prepared following the same procedure but without addition of silver nitrate and ascorbic acid.

2.3. Photocatalytic methodology

The photocatalytic degradation of different azo dyes (Reactive Red 120, Direct Blue 15 and Acid Black 1) was performed using Heber multilamp photoreactor model: HML-COPACT-LP-MP88 (each 8W mercury UV lamp, 365 nm, 4 lamp was used for degradation) [21]. The prepared solution was transferred into a glass tube (2.5 cm -inner diameter and 37 cm – length). The experiment was also conducted under sunlight irradiation. The adsorption-desorption equilibrium was established in the dark condition by suspending the 50 mg of catalysts (CdS and CdS/Ag) in a 100 mL solution that contains 50 ppm (RR 120) of dye molecules. During the experiment, at equal intervals, solutions were collected and centrifuged. The filtered solution was analyzed on a UV–vis spectrometer to measure absorption.

3. Results and discussion

Primary analysis was carried out by RR 120 degradation under UV-A

light with different percentage of Ag loaded CdS materials. About 78, 93 and 88% of degradation observed with 0.5, 1 and 1.5 wt% of Ag loaded CdS, respectively at 120 min irradiation (Fig. S2). Hence, 1 wt% of Ag/CdS was found to be optimum amount of Ag on CdS, and this catalyst has been characterized along with bare CdS for comparison and used for further studies.

3.1. Effect of Ag on the structural property of CdS /Ag nanocomposite

The prepared CdS and CdS/Ag nanocomposites were examined using XRD to confirm the phases and the structures formed. The XRD patterns of CdS and CdS/Ag nanocomposite were depicted in Fig. 1. The obtained pattern reveals the formation of a major phase corresponding to the CdS with hexagonal close-packed structure and P63mc Space Group Symmetry (standard pattern with ref. code no. 00-041-1049 in the PDF4+ database from the ICDD). Other minor peaks can be detected in both XRD patterns. In this case, these peaks seem to correspond to cadmium sulphate hydrate, CdSO₄·H₂O (ref. code no. 00-020-1411 in the PDF4+ database from the ICDD). Anyway, attending to the intensity of peaks, this phase must be in lower amount. In addition, Ag peaks corresponding to the (111) and (220) crystallographic planes were indexed for the CdS/Ag sample, which is due to the loading of Ag. The Ag shows the face centred cubic structure and Fm-3m Space Group Symmetry (standard pattern with ref. no 00-004-0783 in the PDF4+ database from the ICDD). Liu et al. [13], also obtained a similar XRD pattern for the CdS/Ag nanocomposites synthesized by ultrasonic-assisted polyols and hydrothermal methods. However, as it will be later exposed, the microstructure of both CdS/Ag synthesized by Liu et al. and in this work are opposite. The loading of Ag in the CdS influences crystallite size and photocatalytic performance. The crystallite size of the CdS and CdS/Ag nanocomposites was calculated using Scherrer's equation. The average crystallite size of the CdS and CdS/Ag nanoparticles was 34.4 and 28.3 nm, respectively, i.e, around a 18% of crystallite size reduction. This fact can be attributable to the coprecipitation of both phases from the cadmium acetate dihydrate and silver nitrate used as precursor to the CdS/Ag nanoparticles. The deposition of the nano silver (Ag) particles covered the already precipitated CdS nanoparticles can inhibit further growth of them.
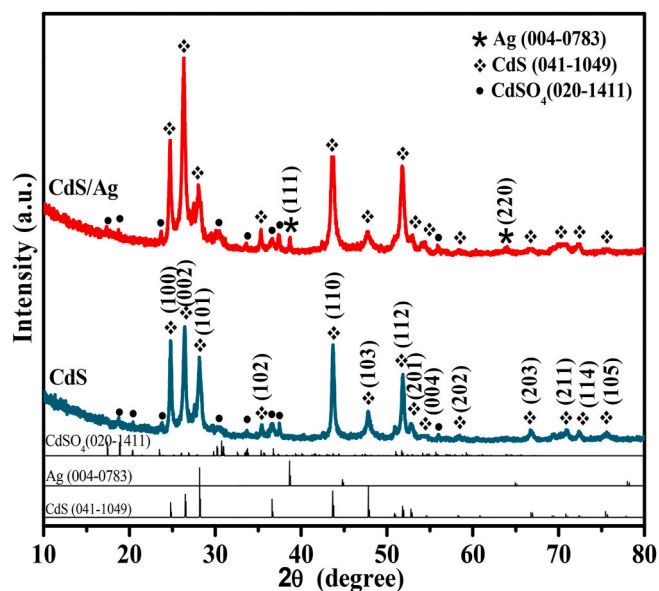

Fig. 1. XRD patterns of CdS and CdS/Ag composite. The indexed phases include the corresponding reference code for the standard pattern of the PDF4+ database from the ICDD.

3.2. Effect of Ag on the vibrational property of CdS/Ag nanocomposite

FT-IR spectroscopy were used to investigate the vibrational property of the prepared nanoparticles, Fig. 2a shows the FT-IR spectra of the CdS and CdS/Ag nanocomposite. The spectra exhibit strong vibration bands at 1552, 1177, 1078, 995 893, 666 and 598 cm^{-1}. The peak at 1552 cm^{-1} represents the bending vibration of –OH bond of water molecule, showing the influence of S, a potential H-bond acceptor that move the peak to a lower wavenumber from a typically ~1600 cm^{-1} [22]. Finally, peaks at 666 and 598 cm^{-1} corresponds to the stretching vibrational bonds of Cd–S [23]. The atomic vibration of the prepared CdS and CdS/Ag nanocomposite was investigated by Raman spectroscopy (Fig. 2b) The spectra clearly show variation in the width of the peaks due to the loading of Ag in the CdS. Again, this aspect is attributable to the decreasing of the crystallinity of CdS because of the Ag loading. The peak present at 302, 603 and 902 cm^{-1} belong to the CdS. The optical phonon mode of the prepared samples was obtained at 302 cm^{-1}. The peak at 603 cm^{-1} was attributed to the first overtone mode of CdS. The second overtone mode of CdS present at 902 cm^{-1}. Swathi and co-authors [24] also observed the first and second-order scattering of the longitudinal optical phonon modes.

3.3. Effect of Ag on the optical property of CdS/Ag nanocomposites

The photoluminescence of the CdS and CdS/Ag nanocomposites was examined and shown in Fig. 3a. The spectra show the higher light emission at 629 nm, and weak emission at 576 nm for both CdS and CdS/Ag nanocomposites. After the loading of Ag, the emission intensity of the CdS is slightly decreases. This confirmed the successful loading of Ag in the CdS. The emission peak at 629 nm is due to the $1s_h$-$1s_e$ excitonic transitions. The broadening of emission peak after Ag loading is owing to the trapping of charge recombination. Also, the size of the particle influences the shifting of PL emission peak [25]. Reddy et al. [26], reported that the emission peak around 629 nm due to the $1s_h$-$1s_e$ excitonic transitions and the variation in PL intensity corresponds to the trapping of charge. This decrease and broadening of the peak enhance the photocatalytic activity of the CdS/Ag nanocomposites.

The optical property of the prepared nanoparticles was studied using DRS-UV Vis. The absorption of the CdS and CdS/Ag nanocomposites is shown in Fig. 3b. After incorporation of Ag with CdS, the absorption of UV and entire visible region increased [27]. The bandgap energy of the CdS and CdS/Ag is calculated using K-M equation [21]. The bandgap energy spectra of the samples are shown in Fig. 3c&d. The bandgap energy of the CdS slightly increased from 2.30 to 2.41 eV after the loading of Ag in the CdS. The bandgap of the Ag incorporated material shows the slightly increased in the bandgap and constructs the transitional levels in the energy gap. Rabizadeh et al. [28], confirmed after silver substitution the formation of the transitional levels in the energy gap. The enhancement in the electron-hole separation results in increased photocatalytic performance.

3.4. Effect of Ag on the morphological property of CdS nanocomposite

SEM and TEM is employed to investigate the morphology of the CdS and CdS/Ag nanocomposite (Figs. 4 and 5, respectively). It reveals that the formation of spherical-shaped nanoparticles in both the CdS and CdS/Ag, and clearly opposite to the morphology found by Liu et al. [13], where it was reported Ag nanowire cores covering by CdS shells. The HR-TEM images of CdS (Fig. 5a), and CdS/Ag (Fig. 5e and g) composites confirmed the formation of spherical-shaped nanoparticles and exhibit that the size of the CdS and CdS/Ag is around 89 and 84 nm, respectively. The corresponding finger print region is given in Fig. 5c and d (CdS), and Fig. 5f and h (CdS/Ag). The d-spacing of the CdS and CdS/Ag is investigated using HR-TEM [29–31]. The obtained d-spacing value of 0.336 nm corresponds to the prominent (002) plane of CdS which is confirmed from the HR-TEM (Fig. 5d, f and h). The SAED pattern of the CdS (Fig. 5b) shows the formation of crystalline nanoparticles. Also, the measured crystallographic distance matches with the XRD (standard pattern no. 00-041-1049 in the PDF4+ database from the ICDD abovementioned) and Raman values. The decrease in the size of the nanoparticles significantly influences the photocatalytic performance of the CdS/Ag. Finally, some Ag nanoparticles could be found in the CdS surface, as can be observed in Fig. 5h (marked by a red circle), where the (111) crystallographic plane was indexed. Due to the nano character of the Ag particles and the low amount (1 wt%), their observations are really difficult to obtain.

3.5. Effect of Ag on the photocatalytic degradation of CdS/Ag nanocomposites

The photocatalytic activity of the CdS and CdS/Ag nanoparticles were investigated towards RR 120, DB 15 and AB 1 under UV and solar light illumination. Figs. S3, S4 and S5 show the degradation of RR 120, DB 15 and AB 1 using CdS and CdS/Ag. These dyes are resistant to self-photolysis [32–34]. Without irradiation, only 21% (RR 120), 18.8 (DB 5) and 22% (AB 1) decrease in dye concentration was observed, and may be due to the adsorption of the dyes on the surface of the catalyst. The photocatalytic activity of the CdS increased for RR 120, DB 15 and AB 1 under UV and solar light illumination after incorporation of Ag into the CdS. The substitution of Ag greatly increases the photocatalytic dye
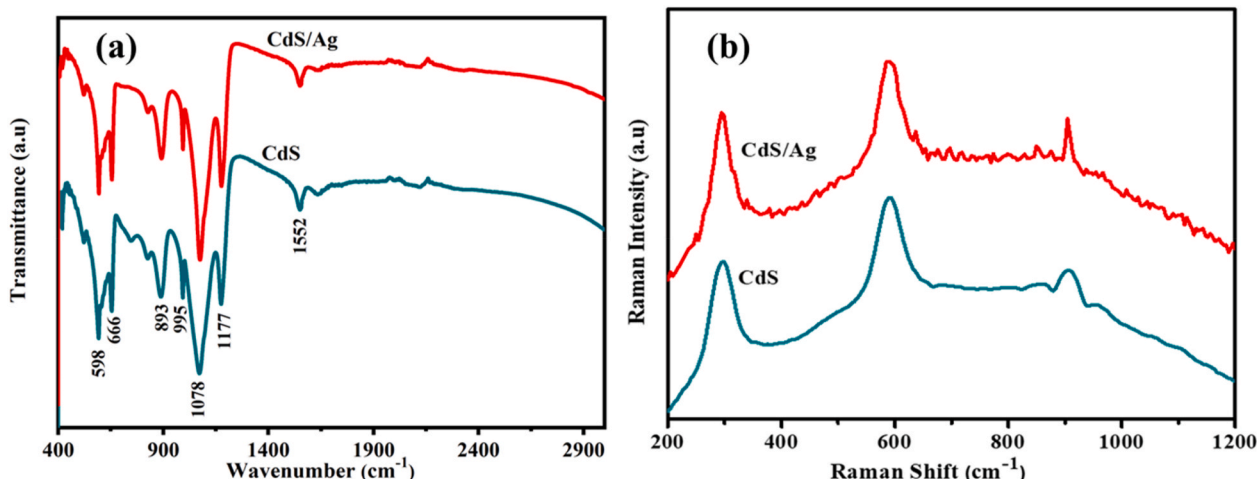

Fig. 2. FT-IR (a) and Raman (b) spectra of CdS and CdS/Ag nanocomposite.
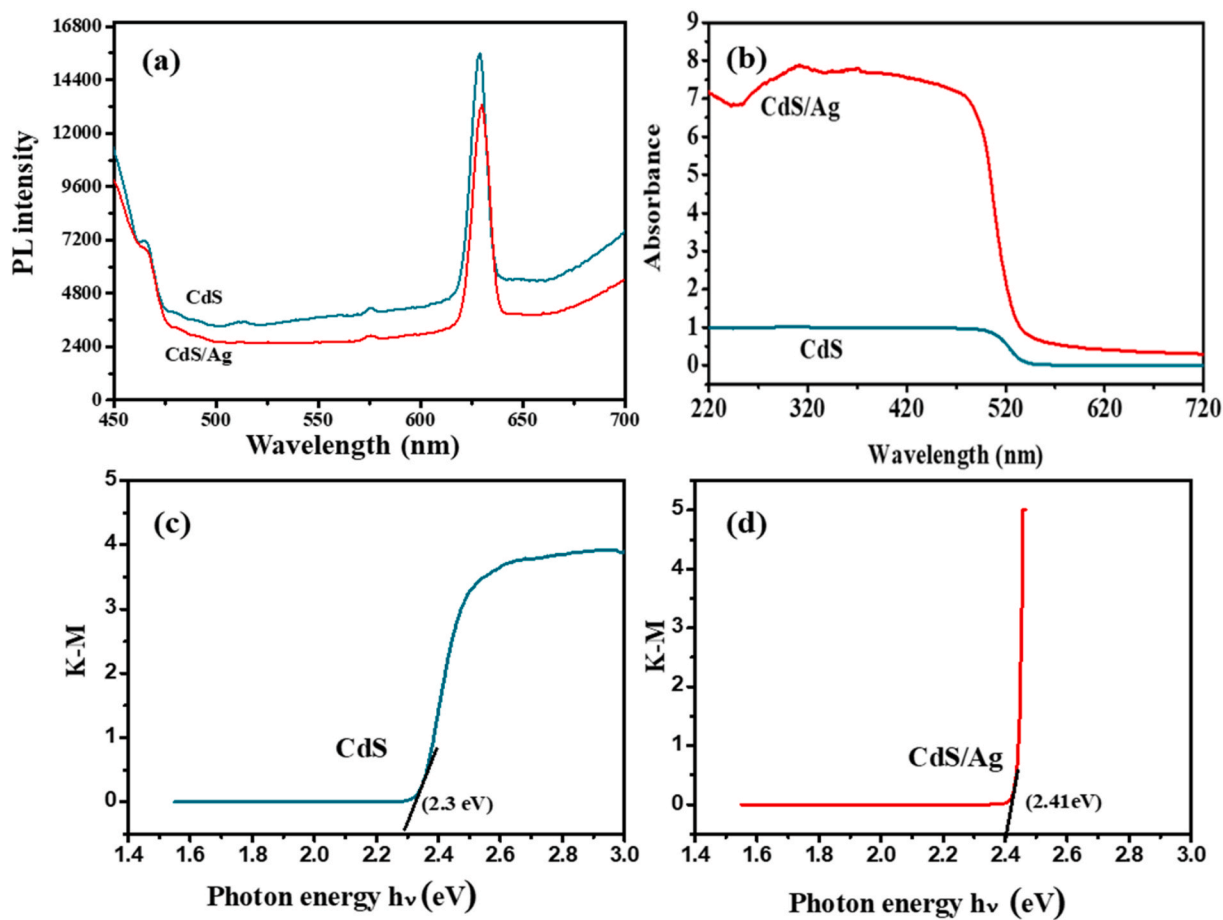
Fig. 3. PL (a), DRS (b), K. M plots (c& d) of CdS and CdS/Ag nanocomposite.
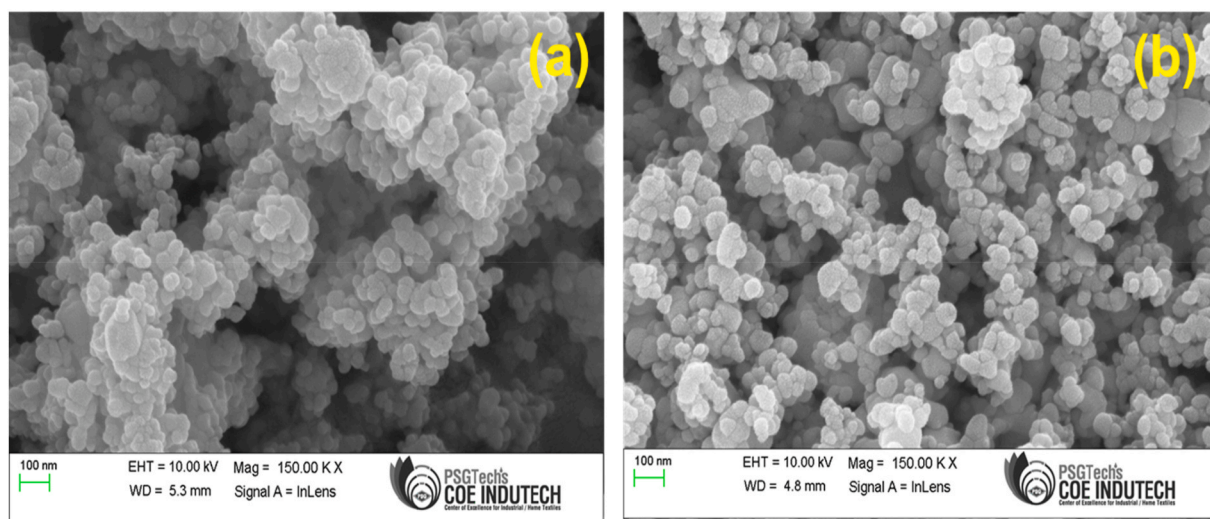

Fig. 4. FE-SEM images of (a) CdS and (b) CdS/Ag nanocomposite.

removal efficiency of CdS. The photocatalytic degradation percentage of CdS shows 70, 64 and 73%, whereas CdS/Ag removed more than 95% dye of molecules in solar light. The CdS/Ag catalysts show higher photocatalytic activity in the presence of sunlight and UV light irradiation. The substitution of Ag greatly influences the carrier charge separation and increases the photocatalytic activity (Fig. 6a) [35]. The reaction of kinetic properties of photodegradation in different azo dye using CdS and CdS/Ag nanocomposite was assessed by *pseudo*-first-order kinetics

equation (1) [36,37].

$$\ln(C_0 / C_t) = kt \tag{1}$$

Where C_o – initial concentration of dye solution, C_t - concentration of dye at time t, t – degradation time and k - apparent rate constant. The plot of $\ln(C_0 / C_t)$ vs. treatment time t is given in Fig. 6b. Besides, CdS/Ag improved the degradation rate of the photocatalyst and composite with
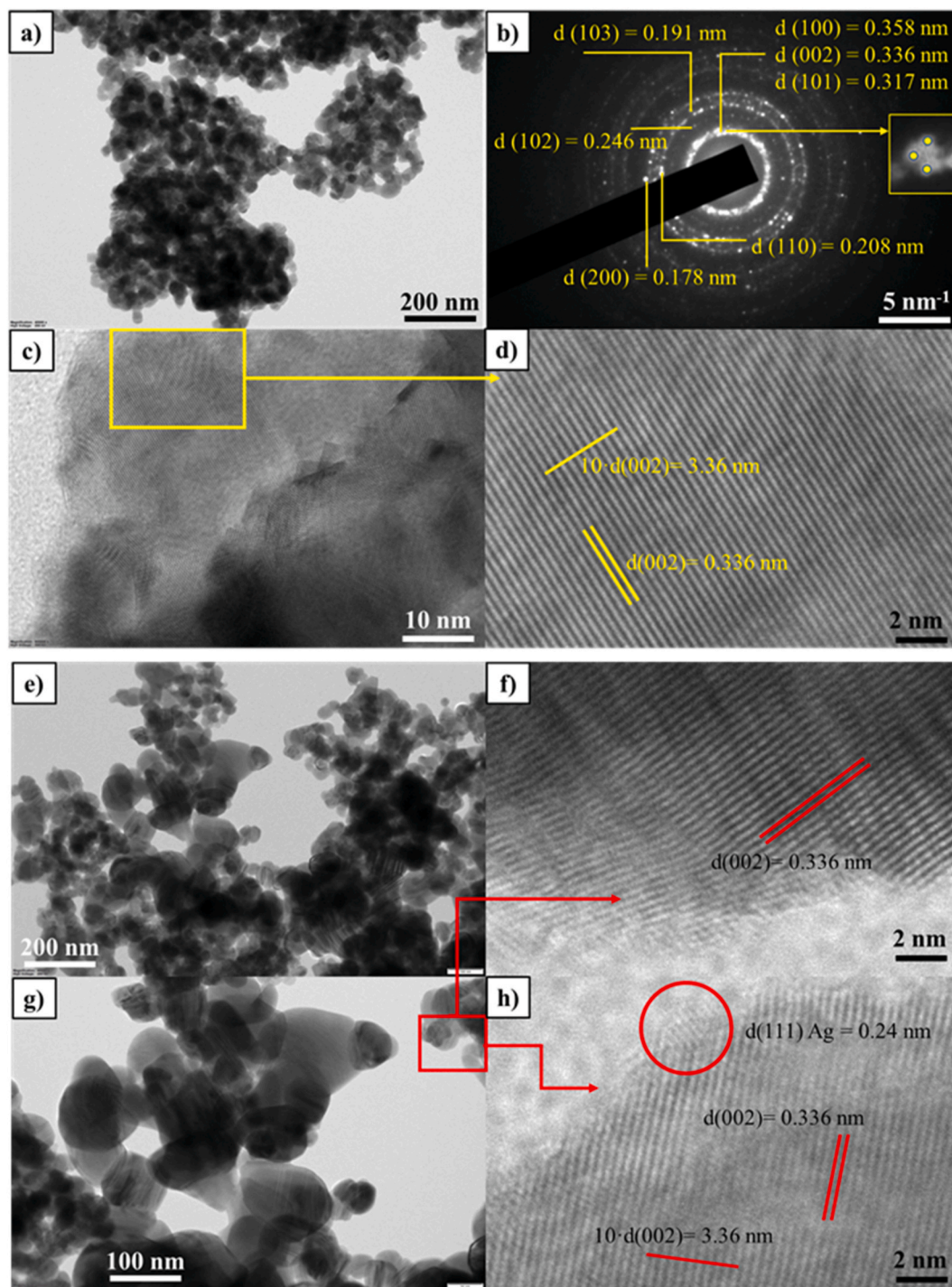
Fig. 5. HRTEM and SAED images for the CdS (a–d) and CdS/Ag (e–h) nanocomposite.

Ag. Table 1 shows the kinetic results of CdS and CdS /Ag towards Reactive Red 120, Direct Blue 15 and Acid Black 1. The rate constants of CdS/Ag are higher than CdS. Furthermore, the reusability of CdS/Ag remains at a high level even at fourth cycle (discussion comes later), which indicates that the CdS/Ag is highly stable.

The mechanism of the degradation of RR 120, DB 15 and AB 1 by CdS/Ag under solar and UV light is shown in Fig. 7a. The two-component system (CdS and Ag) is effectively involved in the degradation process. The valence band (VB) and conduction band (CB) edge potentials of CdS were estimated via Mulliken electronegativity theory [38], and found to be +1.937 and −0.363 eV, respectively. The CdS under UV/sunlight irradiation, the electrons are excited to the conduction band (CB) and leave a hole in the valence band (VB). Since CdS is a semiconductor and acts as photoactive center. The photo-excited electrons were trapped by Ag particles and react with dissolved oxygen produced superoxide radical anions ($O_2^{\bullet -}$) [39]. At the same time, the holes in the valence band react with water to form hydroxyl radicals ($^{\bullet}OH$). Due the presence of noble metals of Ag, a greater number of electrons were trapped from CB of CdS results reduce the electron-hole recombination significantly and enhance the photocatalytic activity of the material.

3.5.1. Effects of scavengers on degradation (RR 120) efficiency

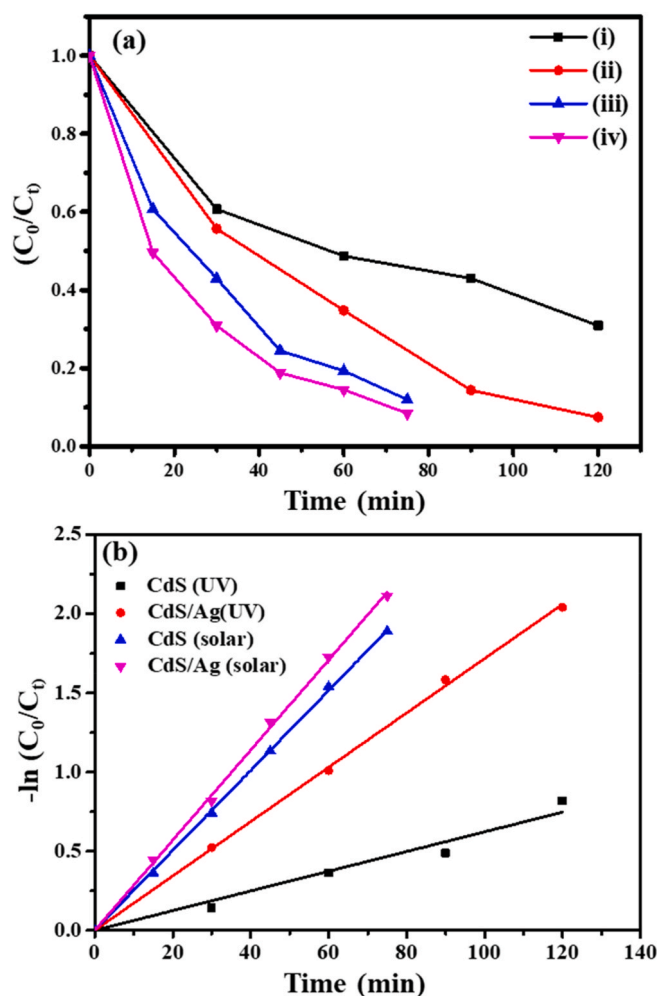The most active species involved in the photodegradation process

Fig. 6. Photodegradability of RR 120 (a) UV light (i) CdS, (ii) CdS/Ag and Solar light (iii) CdS, (iv) CdS/Ag at pH 5; (b) Corresponding Kinetic plots for the photodegradation of RR 120.

Table 1
Kinetic values in the photodegradation of different catalysts.

Catalyst Name	Reactive Red 120		Direct Blue 15		Acid Black 1	
	k (min^{-1})	R^2	k (min^{-1})	R^2	k (min^{-1})	R^2
UV-A light						
CdS	0.0062	0.9955	0.0236	0.98483	0.0248	0.9859
CdS/Ag	0.0171	0.9996	0.0500	0.99021	0.0431	0.9987
Solar light						
CdS	0.0252	0.9983	0.0406	0.9940	0.0433	0.9966
CdS/Ag	0.0284	0.9995	0.0566	0.9974	0.0721	0.9912

(solar) with CdS/Ag nanocomposite were investigated by the trapping experiment and the results is shown in Fig. 7b. The addition of 1 mmol of tertiary butyl alcohol (TBA, •OH scavenger), silver nitrate (AgNO$_3$, e$^-$ scavenger), benzoquinone (BQ, O$_2^{•-}$ scavenger) and potassium iodide (KI, h$^+$ scavenger) play a significant reduction in the photodegradation efficiently of the catalyst. Without scavenger, about 93% of degradation observed at 75 min. At the same time, addition of TBA, AgNO$_3$, BQ and KI gave 34, 24, 19 and 17 percentages of degradations, respectively. Among the scavengers, the addition of KI was significantly reducing the catalytic activity and revealed that h$^+$ are the main active species in this degradation. The active species contributes the following order h$^+$ > O$_2^{•-}$ > e$^-$ > •OH.

3.5.2. Effect of initial dye pH on degradation and mineralization of dyes

The industrial effluents are usually coming with a wide range of pH. It is imperative to treat the effluent without alter the pH, which could be a cost-effective and energy-efficient process for water remediation. In this point of view, the influence of pH on photocatalytic activity of RR 120 towards CdS/Ag were studied under UV and solar light which is shown in Fig. 8a and values are tabulated in Table 2. The photocatalytic degradation of organic dye molecules strongly depends on the pH of the solution and for selected test dye molecules, the pH is 5. Table 2 confirms that the CdS/Ag shows higher removal of dye in the pH 5. Below and above the pH 5, degradation ability is less both UV and solar light. Almost the same trend was observed in all the catalysts. When compared with CdS modified samples show effective degradation in all the pH. The
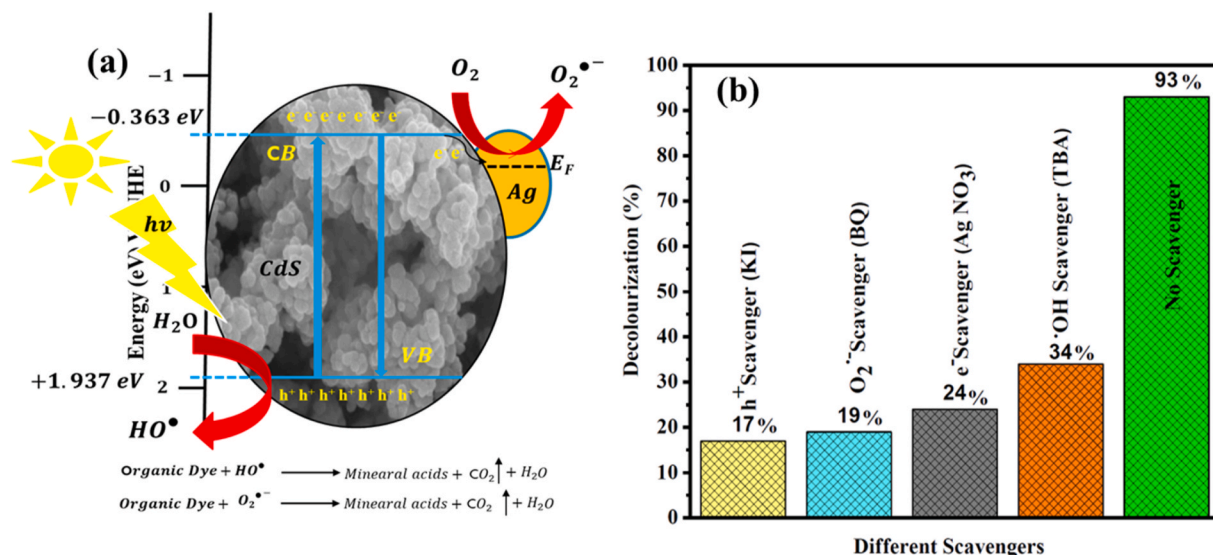
Fig. 7. (a) Mechanism of photocatalytic dye degradation of dyes with CdS/Ag and (b) Effects of scavengers on degradation (RR 120) efficiency by CdS/Ag.
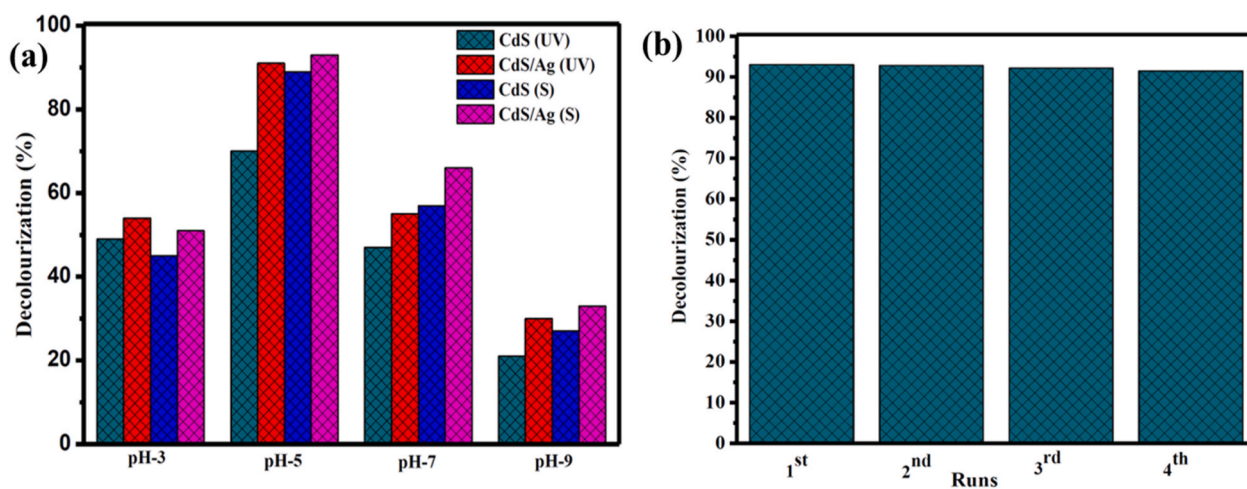

Fig. 8. (a) Effect of pH on RR 120 decolourization by CdS and CdS/Ag UV and Solar light, [RR 120] = 50 ppm; catalyst suspended = 50 mg/100 mL. (b) Catalysts reusability on photocatalytic decolourization of RR 120 dye under UV light irradiation, [RR 120] = 50 ppm; CdS/Ag and suspended catalyst = 50 mg/100 mL; irradiation time = 120 min at pH 5.

prepared CdS/Ag is efficient towards RR120 degradation in UV and solar light irradiation.

To verify the complete mineralization process, Chemical Oxygen Demand (COD) was determined based on the reported procedure [40]. The percentage of COD reductions of these three dyes (RR 120, DB 15 and AB 1) at different time of irradiation under optimized pH condition in UV A light are presented in Table S1. About 80% (RR 120), 82% (DB 15) and 86% (AB 1) of COD reductions were observed for these dyes under optimized conditions. This study confirm that the dyes underwent almost complete degradation and mineralized.

3.5.3. Reusability of CdS/Ag nanocomposite towards RR120

The reusability of the CdS/Ag nanoparticles was studied towards RR120. The experimental parameter was fixed (pH = 5, irradiation time-120 min, catalyst = 50 mg/100 mL and the dye = 50 ppm) and shown in Fig. 8b. In the fixed reaction contagion, the prepared CdS/Ag shows at least a 90% stability after 4th cycle. This result confirms prepared material is efficient in removing the organic dye molecule. The stability of the prepared CdS/Ag is higher, which is due to the substitution of Ag.

Also, a decrease in the size, and photoluminescence famous for the photocatalytic degradation and stability of the silver substituted CdS composite.

3.6. Comparison of efficiency of CdS/Ag with modified CdS based photocatalysts

The efficiency of synthesized CdS/Ag composite was compared [41–45] with modified CdS based photocatalyst which were utilized for pollutant degradation under various conditions (Table 3). Although, the present investigation has been varied with catalyst dosage, degradation time, initial pH of the pollutant, concentration of the pollutant, light source, the comparison can give some idea about the efficiency of the synthesized materials with other reported CdS based materials. From Table 3, the composite catalyst reported here was effective in degradation of three toxic dyes (RR 120, DB 15 and AB1) under UV as well as in direct sunlight irradiation. In all the processes, >90% of degradation was achieved.

Table 2
Effect of pH on degradation of different dyes with CdS and CdS/Ag.

Catalyst Name	Reactive Red 120 (%)				Direct Blue 15 (%)				Acid Black 1 (%)			
	pH-3	pH-5	pH-7	pH-9	pH-3	pH-5	pH-7	pH-9	pH-3	pH-5	pH-7	pH-9
UV-A (light)												
CdS	49	70	47	21	49	67	44	27	51	73	43	23
CdS/Ag	54	93	55	30	58	94	50	32	57	95	52	31
Solar (light)												
CdS	45	89	57	27	50	80	54	29	58	82	61	31
CdS/Ag	51	93	66	33	59	92	63	35	65	92	66	40

Table 3
A comparison of CdS/Ag efficiency with other reported modified CdS based photocatalysts.

S. No	Catalysts	Pollutants/Light used	Concentration	Catalyst amount	% of degradation/time (min)	References
1	Ag/CdS	Methylene Blue (MB)/Visible light, (500 W halogen lamp)	10 ppm	30 mg/200 mL	95.35/240	[13]
2	CuO/CdS	Rhodamine B (RhB)/Visible light, (500 W Xenon lamp)	30 ppm	75 mg/100 mL	93/60	[41]
3	PANI/CdS	Rhodamine B (RhB)/Visible light, halogen lamp (150 W)	25 ppm	100 mg/200 mL	99/60	[42]
4	CdS/GO/ZnO	Methyl Orange (MO), Visible light, 400 W metal halide lamp	20 ppm	50 mg/-	>90/120	[43]
5	Zn/CdS	Rhodamine B (RhB)/UV, Xenon arc lamp	5 ppm	20 mg/100 mL	85/135	[44]
6	Zn/CdS	Rhodamine B (RhB)/Solar light	5 ppm	20 mg/100 mL	93/135	[44]
7	CdMoO$_4$@CdS	Malachite Green/Visible light (1 kW xenon lamp)	30 ppm	20 mg/50 mL	90/120	[45]
8	CdS/Ag	Reactive Red 120 (RR 120, 8W mercury UV lamp, 365 nm/direct sunlight	50 ppm	50 mg/100 mL	93/120[a] and 93/75[b]	Present work
9	CdS/Ag	Direct Blue 15 (DB 15), 8W mercury UV lamp, 365 nm/direct sunlight	10 ppm	10 mg/100 mL	94/50[a] and 92/35[b]	Present work
10	CdS/Ag	Acid Black 1 (AB 1), 8W mercury UV lamp, 365 nm/direct sunlight	10 ppm	10 mg/100 mL	95/50[a] and 92/30[b]	Present work

[a] Degradation carried out under UV-A light.
[b] Degradation carried out under direct sunlight.

4. Conclusions

Spherical shaped morphologies CdS/Ag nanoparticles were obtained by co-precipitation method, confirmed by SEM and TEM studies. XRD and Raman analysis reveals the formation of CdS with Ag at the particle surface. The significant shift in the PL emission and UV absorption is due to the Ag loading. The decrease in the bandgap and size of the nanoparticles traps the charge recombination and enhances the degradation efficiency against the different organic dye molecules. The photocatalysts efficient in the photodegradation of RR 120, DB 15 and AB 1 dye under UV and sun light and CdS/Ag system was higher compared to bare CdS. The CdS/Ag catalyst is stable after 4th cycle and shows 93% of degradation without any scavengers. This confirms the prepared CdS/Ag catalyst will be useful for the degradation of organic pollutants.

Author contribution

S. Ravikumar: Experimental section and writing first draft. **Mani Durai**: Conceptualization, methodology, and editing. **E. Chicardi**: Software, data curation, and XRD discussion. **R. Sepúlveda**: Software, writing-review, and FT-IR discussion. **Krishnakumar Balu**: Materials synthesis, conceptualization, supervision, writing–review, and editing. **V. Pandiyan**: Conceptualization, supervision, writing–review, and editing. **Young-Ho Ahn**: Conceptualization, writing–review, and editing.

Declaration of competing interest

The authors declare that they have no known competing financial interests or personal relationships that could have appeared to influence the work reported in this paper.

Appendix A. Supplementary data

Supplementary data to this article can be found online at https://doi.org/10.1016/j.ceramint.2022.11.123.

References

[1] J.A. Scher, J.M. Elward, A. Chakraborty, Shape matters: effect of 1D, 2D, and 3D isovolumetric quantum confinement in semiconductor nanoparticles, J. Phys. Chem. C 120 (2016) 24999–25009.

[2] D. Lv, D. Zhang, X. Pu, D. Kong, Z. Lu, X. Shao, H. Ma, J. Dou, One-pot combustion synthesis of BiVO$_4$/BiOCl composites with enhanced visible-light photocatalytic properties, Separ. Purif. Technol. 174 (2017) 97–103.

[3] Z. Fang, L. Zhang, T. Yang, L. Su, K.C. Chou, X. Hou, Cadmium sulfide with tunable morphologies: preparation and visible-light driven photocatalytic performance, Phys. Met.: Low-Dimens. Syst. Nanostructures 93 (2017) 116–123.

[4] Y. Zheng, X. Hou, Q. Li, Z. Fang, T. Yang, T. Liang, X. Duan, M. Shang, W. Yang, Electrostatic interaction assistant synthesis of CdS/BCN heterostructure with enhanced photocatalytic effect, J. Mater. Chem. C 8 (2020) 1803–1810.

[5] T. Wu, G. Liu, J. Zhao, H. Hidaka, N. Serpone, Photoassisted degradation of dye pollutants. V. Self-photosensitized oxidative transformation of rhodamine B under visible light irradiation in aqueous TiO$_2$ dispersions, J. Phys. Chem. B 102 (1998) 5845–5851.

[6] R. Georgekutty, M.K. Seery, S.C. Pillai, A highly efficient Ag-ZnO photocatalyst: synthesis, properties, and mechanism, J. Phys. Chem. C 112 (2008) 13563–13570.

[7] T. Senasu, T. Chankhanittha, K. Hemavibool, S. Nanan, Visible-light-responsive photocatalyst based on ZnO/CdS nanocomposite for photodegradation of reactive red azo dye and ofloxacin antibiotic, Mater. Sci. Semicond. Process. 123 (2021), 105558.

[8] H. Yu, Y. Huang, D. Gao, P. Wang, H. Tang, Improved H2-generation performance of Pt/CdS photocatalyst by a dual-function TiO$_2$ mediator for effective electron transfer and hole blocking, Ceram. Int. 45 (2019) 9807–9813.

[9] K. Deka, M.P. Kalita, Structural phase controlled transition metal (Fe, Co, Ni, Mn) doping in CdS nanocrystals and their optical, magnetic and photocatalytic properties, J. Alloys Compd. 757 (2018) 209–220.

[10] J.-C. Wu, J. Zheng, P. Wu, R. Xu, Study of native defects and transition-metal (Mn, Fe Co, and Ni) doping in a zinc-blende CdS photocatalyst by DFT and hybrid DFT calculations, J. Phys. Chem. C 115 (2011) 5675–5682.

[11] Y.-J. Jing, L. Kang, CdS nanoparticles decorated Ag$_2$WO$_4$ nanorods for increased photocatalytic performance and stability under visible light irradiation, Ceram. Int. 46 (2020) 18826–18831.

[12] B. Xin, L. Jing, Z. Ren, B. Wang, H. Fu, Effects of simultaneously doped and deposited Ag on the photocatalytic activity and surface states of TiO$_2$, J. Phys. Chem. B 109 (2005) 2805–2809.

[13] Y. Liu, M. Chi, H. Dong, H. Jia, B. Xu, Z. Zhang, Ag/CdS heterostructural composites: fabrication, characterizations and photocatalysis, Appl. Surf. Sci. 313 (2014) 558–562.

[14] L. Bai, X. Wang, S. Tang, Y. Kang, J. Wang, Y. Yu, Z.-K. Zhou, C. Ma, X. Zhang, J. Jiang, Black phosphorus/platinum heterostructure: a highly efficient photocatalyst for solar-driven chemical reactions, Adv. Mater. 30 (2018), 1803641.

[15] X. Hu, Y. Li, J. Tian, H. Yang, H. Cui, Highly efficient full solar spectrum (UV-vis-NIR) photocatalytic performance of Ag$_2$S quantum dot/TiO$_2$ nanobelt heterostructures, J. Ind. Eng. Chem. 45 (2017) 189–196.

[16] N. Zhang, X. Li, Y. Wang, B. Zhu, J. Yang, Fabrication of magnetically recoverable Fe$_3$O$_4$/CdS/g-C$_3$N$_4$ photocatalysts for effective degradation of ciprofloxacin under visible light, Ceram. Int. 46 (2020) 20974–20984.

[17] S. Huang, Y. Lin, J. Yang, X. Li, J. Zhang, J. Yu, H. Shi, W. Wang, Y. Yu, Enhanced photocatalytic activity and stability of semiconductor by Ag doping and simultaneous deposition: the case of CdS, RSC Adv. 3 (2013) 20782–20792.

[18] P. Dhiman, N. Dhiman, A. Kumar, G. Sharma, M. Naushad, A.A. Ghfar, Solar active nano-Zn1−xMgxFe$_2$O$_4$ as a magnetically separable sustainable photocatalyst for degradation of sulfadiazine antibiotic, J. Mol. Liq. 294 (2019), 111574.

[19] S.J. Lee, T. Begildayeva, H.J. Jung, R. Koutavarapu, Y. Yu, M. Choi, M.Y. Choi, Plasmonic ZnO/Au/g-C3N4 nanocomposites as solar light active photocatalysts for degradation of organic contaminants in wastewater, Chemosphere 263 (2021), 128262.

[20] B. Krishnakumar, R. Velmurugan, B. Subash, M. Swaminathan, Mineralization of genotoxic acid violet 7 by AgBr-ZnO under alkaline conditions using direct sunlight, Indian J. Chem. 51A (2012) 580–585.

[21] S. Ravikumar, V. Pandiyan, M. Alam, N. Ahmad, V. Nithya, B. Krishnakumar, A. J. Sobral, Costus speciosus koen leaf extract assisted CS-ZnX (X= O or S) nanomaterials: synthesis, characterization and photocatalytic degradation of RR 120 dye under UV and direct sunlight, J. Mol. Struct. 1225 (2021), 129176.

[22] N. Susha, K. Nandakumar, S.N. Swapna, Enhanced photoconductivity in CdS/betanin composite nanostructures, RSC Adv. 8 (2018) 11330–11337.

[23] T. Iqbal, G. Ara, N.R. Khalid, M. Ijaz, Simple synthesis of Ag-doped CdS nanostructure material with excellent properties, Appl. Nanosci. 10 (2020) 23–28.

[24] S. Swathi, R. Yuvakkumar, G. Ravi, E.S. Babu, D. Velauthapillai, A. Syed, T. M. Dawoud, Silver-doped cadmium sulfide for electrochemical water oxidation, Appl. Nanosci. 10 (2020) 4351–4358.

[25] C.Z. Wang, Y. E, L.Z. Fan, Z.H. Wang, H.B. Liu, Y.L. Li, S.H. Yang, Y.L. Li, Directed assembly of hierarchical CdS nanotube Arrays from CdS nanoparticles: enhanced solid state electro-chemiluminescence in H$_2$O$_2$ solution, Adv. Mater. 19 (2007) 3677–3681.

[26] M.P. Reddy, B.C. Jamalaiah, I.G. Kim, D.S. Yoo, R.R. Reddy, A convenient noninjection one-pot synthesis of CdS nanoparticles and their studies, Adv. Mater. Lett. 4 (2012) 621–625.

[27] Y.-J. Hsu, S.-Y. Lu, Dopant-Induced formation of branched CdS nanocrystals, Small 4 (2008) 951–955.

[28] H. Rabizadeh, A. Feizbakhsh, H. Ahmad Panahi, E. Konoz, Synthesis and characterization of Ag doped cadmium sulfide/multi walled carbon nanotubes: structural, and photocatalysis studies, Fullerenes, Nanotub. Carbon Nanostruct. 27 (2019) 788–795.

[29] N.E. Fard, R. Fazaeli, R. Ghiasi, Band gap energies and photocatalytic properties of CdS and Ag/CdS nanoparticles for Azo dye degradation, Chem. Eng. Technol. 39 (2016) 149–157.

[30] G. Lin, J. Zheng, R. Xu, Template-free synthesis of uniform CdS hollow nanospheres and their photocatalytic activities, J. Phys. Chem. C 112 (2008) 7363–7370.

[31] H.R. Liu, G.X. Shao, J.F. Zhao, Z.X. Zhang, Y. Zhang, J. Liang, X.G. Liu, H.S. Jia, B. S. Xu, Worm-like Ag/ZnO core–shell heterostructural composites: fabrication, characterization, and photocatalysis, J. Phys. Chem. C 116 (2012) 16182–16190.

[32] B. Krishnakumar, M. Swaminathan, Solar photocatalytic degradation of naphthol blue black, Desalination Water Treat. 51 (2013) 6572–6579.

[33] B. Subash, B. Krishnakumar 1, M. Swaminathan, M. Shanthi, β-Ag$_2$S–ZnO as a novel sunshine photocatalyst for the effective degradation of RR 120 dye, Powder Technol. 241 (2013) 49–59.

[34] U. Rajaji, S.E.G. Dhana Rani, S.M. Chen, K. Rajakumar, M. Govindasamy, F. M. Alzahrani, N.S. Alsaiari, M. Ouladsmane, I.S. Lydia, Synergistic photocatalytic activity of SnO$_2$/PANI nanocomposite for the removal of direct blue 15 under UV light irradiation, Ceram. Int. 47 (2021) 29225–29231.

[35] C. Xu, L. Cao, G. Su, W. Liu, X. Qu, Y. Yu, Preparation, characterization and photocatalytic activity of Co-doped ZnO powders, J. Alloys Compd. 497 (2010) 373–376.

[36] R. Tanwar, S. Kumar, U.K. Mandal, Photocatalytic activity of PANI/Fe^0 doped BiOCl under visible light-degradation of Congo red dye, J. Photochem. Photobiol., A 333 (2017) 105–116.

[37] Y. Wang, G. Meng, L. Zhang, C. Liang, J. Zhang, Catalytic growth of large-scale single-crystal CdS nanowires by physical evaporation and their photoluminescence, Chem. Mater. 14 (2002) 1773–1777.

[38] B. Krishnakumar, R. Hariharan, V. Pandiyan, António Aguiar, Abilio J.F.N. Sobral, Gelatin-assisted g-TiO$_2$/BiOI heterostructure nanocomposites for azo dye degradation under visible light, J. Environ. Chem. Eng. 6 (2018) 4282–4288.

[39] P. Gnanamozhi, V. Renganathan, S.-M. Chen, V. Pandiyan, M.A. Arockiaraj, N. S. Alharbi, S. Kadaikunnan, J.M. Khaled, K.F. Alanzi, Influence of Nickel concentration on the photocatalytic dye degradation (methylene blue and reactive red 120) and antibacterial activity of ZnO nanoparticles, Ceram. Int. 46 (2020) 18322–18330.

[40] B. Subash, Balu Krishnakumar, Abilio J.F.N. Sobral, C. Surya, N. Agnel Arul John, A. Senthilraja, M. Swaminathan, M. Shanthi, Synthesis, characterization and daylight active photocatalyst with antiphotocorrosive property for detoxification of azo dyes, Separ. Purif. Technol. 164 (2016) 170–181.

[41] S.S. Hossain, M. Tarek, T.D. Munusamy, K.M.R. Karim, S.M. Roopan, S.M. Sarkar, C.K. Cheng, M.M. Rahman Khan, Facile synthesis of CuO/CdS heterostructure hotocatalyst for the effective degradation of dye under visible light, Environ. Res. 188 (2020), 109803.

[42] S. Sharma, D. Kumar, N. Khare, Hierarchical PANI/CdS nanoarchitecture system for visible light induced photocatalytic dye degradation and photoelectrochemical water splitting, Polymer 231 (2021), 124117.

[43] D. Das, P. Nandi, Synthesis of CdS/GO modified ZnO heterostructure for visible light dye degradation applications, Appl. Surf. Sci. 570 (2021), 151260.

[44] A. Singh, D. Singh, B. Ahmed, A.K. Ojha, Sun/UV-light driven photocatalytic degradation of rhodamine B dye by Zn doped CdS nanostructures as photocatalyst, Mater. Chem. Phys. 277 (2022), 125531.

[45] C. Zhang, T. Zhang, Y. Wang, Q. Liang, M. Zhou, X. Li, Z. Li, S. Xu, In-situ synthesis of 3D CdMoO$_4$@CdS core-shell structure for efficient photocatalytic degradation, Ceram. Int. 48 (2022) 15064–15072.